

# IMPROVED SEGMENTATION OF FOCAL CORTICAL DYSPLASIA LESIONS ON MRI USING EXPANSION TOWARDS CORTICAL BOUNDARIES

*O. Colliot, T. Mansi, P. Besson, N. Bernasconi, A. Bernasconi*

McConnell Brain Imaging Center, Montreal Neurological Institute,  
McGill University, Montreal, Canada

## ABSTRACT

Focal cortical dysplasia (FCD), a malformation of cortical development, is an important cause of intractable epilepsy. On Magnetic Resonance Images (MRI), FCD lesions are difficult to distinguish from healthy cortex and defining their spatial extent is challenging. We previously introduced a method to segment FCD lesions on MRI, relying on a 3D deformable model driven by MR features of FCD. In the present paper, we propose to improve our approach by adding a second evolution step which expands the result towards the cortical boundaries. A quantitative evaluation was performed in 18 FCD patients by comparison with manually traced lesion labels. The proposed approach achieved a strong agreement with the manual labels and substantially improved the results obtained with our previous method.

## 1. INTRODUCTION

Focal cortical dysplasia (FCD) [1], a malformation of cortical development, is an important cause of medically intractable epilepsy. Epilepsy surgery, consisting in the removal of the FCD lesion, can lead to seizure freedom. However, the prognosis is poorer than in patients operated for other types of lesions. Unfavorable outcomes may be due to incomplete resection of the lesion [2].

High-resolution magnetic resonance imaging (MRI) has allowed the recognition of FCD in an increased number of cases. However, the spatial extension of FCD lesions is difficult to define on the MRI as the lesions are often subtle, not easily differentiable from the normal cortex and with ill-defined boundaries. The precise delineation of lesions on MRI could lead to more complete excision and better surgical outcome. It is thus an important issue for surgical planning.

Voxel-based techniques have been developed for detection of FCD on MRI [3, 4, 5]. In particular, computational models of FCD characteristics [6] and a Bayesian classifier for lesion detection [4] were previously proposed by our group. While these approaches successfully identify the FCD in a

majority of patients, they cover a small fraction (about 20%) of the lesion extent and thus cannot be used for delineation.

We recently proposed a method for segmenting FCD lesions on T1-weighted MRI [7]. This approach, which we called feature-based deformable model (FDM), relied on a 3D level set driven by feature maps representing known MR characteristics of FCD. We demonstrated a good agreement between automatic segmentations and two sets of manual labels. To our knowledge, apart from our previous study, the question of FCD segmentation has never been addressed.

Histological studies have shown that, in FCD, all cortical layers, from the outer part of the cortex to the junction with the white matter, are affected by the pathology [8]. This suggests that FCD lesions are not limited to regions exhibiting abnormal MR features but should extend over the entire cortical section, which was not fully covered by the feature-based deformable model. In the present paper, we propose to improve our previous method by adding a second evolution step to expand the result obtained with the FDM towards the underlying and overlying cortical boundaries, throughout the whole cortical section. On the contrary, intra-cortical motion in the lateral direction will be prevented in order to avoid progressing into the neighboring healthy cortex.

## 2. METHODS

### 2.1. Previous work: feature-based deformable model

Here, we briefly recall the underlying principles of our previous feature-based deformable model for FCD segmentation. More details can be found in [7].

The deformable model was driven by a probability map derived from three FCD features. These features correspond to known visual characteristics of FCD on T1-weighted MRI and were evaluated using our previous computational models [6], resulting in three feature maps:

- a cortical thickness map, denoted as  $Th$ , to identify areas of focal cortical thickening,
- a relative intensity map ( $RI$ ) to emphasize hyper-intense signal within the dysplastic lesion,
- a gradient map ( $Gr$ ) to model blurred transitions between gray and white matter.

---

This work was supported by the Canadian Institutes of Health Research (CIHR grant 203707) and the Scottish Rite Charitable Foundation of Canada. OC is recipient of the Epilepsy Canada Clinical Sciences Fellowship.

These three characteristics defined a vector-valued feature map  $f(x) = (Th(x), RI(x), Gr(x))$  at each point  $x$  in the image space. Then, a supervised learning was performed on a training set of patients in order to estimate the probabilities  $P(c|f(x))$  of four tissue classes  $c$  - cerebrospinal fluid (CSF), gray matter (GM), white matter (WM), and FCD lesion (L) - given the feature vector  $f$ .

The 3D deformable model was designed as a region competition between the lesion and the most probable non-lesional class. The motion of a point  $u$  belonging to the interface  $S$  of the lesion was then defined as:

$$\frac{\partial u}{\partial t} = \alpha_1 [R_{NL}(u) - R_L(u)] \mathbf{n}_u + \epsilon_1 \kappa_u \mathbf{n}_u \quad (1)$$

where  $R_L(x) = P(L|f(x))$  is a term attached to the lesion,  $R_{NL}(x) = \max\{P(GM|f(x)), P(WM|f(x)), P(CSF|f(x))\}$  is a term attached to the healthy tissues,  $\mathbf{n}_u$  is the inward normal to  $S$  at point  $u$  (directed towards the interior of the lesion),  $\kappa_u$  is the mean curvature and  $\alpha_1$  and  $\epsilon_1$  are weighting coefficients.

To initialize the level set, we used our previously developed FCD classifier [4], under supervision.

## 2.2. Expansion towards cortical boundaries

To drive the second deformable model towards the boundaries of the cortex, we relied on a gradient vector flow (GVF) [9], computed from the GM segmentation. The GVF is computed by diffusion of the gradient vector and provides a smooth vector field which is approximately orthogonal to the GM boundaries. An example of GVF is shown in Figure 1.

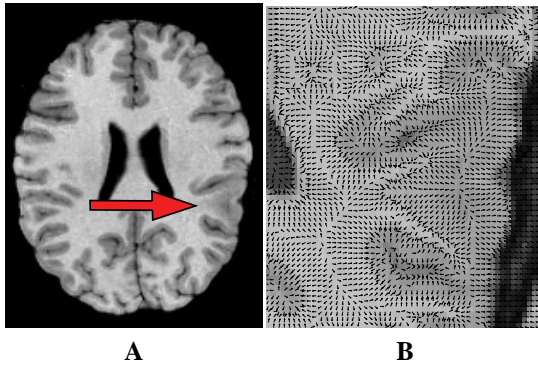


**Fig. 1.** Computation of the gradient vector flow (GVF) in a patient with FCD. (A) T1-weighted MRI where the FCD lesion is indicated by the arrow. (B) Detail of the normalized GVF in the region of the lesion.

The following force was used to drive the deformable model towards the cortical boundaries using the GVF:

$$\mathbf{F}_{GVF} = [\hat{\mathbf{v}}(u) \cdot \mathbf{n}_u] \mathbf{n}_u \quad (2)$$

where  $\mathbf{n}_u$  is the inward normal to the surface at point  $u$ ,  $\hat{\mathbf{v}}(u)$  is the normalized GVF and  $\cdot$  is the scalar product.

This force enables the model to progress in a direction orthogonal to the cortical boundaries while avoiding lateral motion. When the normal to the surface is oriented along the GVF,  $F = \|\mathbf{F}_{GVF}\| > 0$  and the surface is attracted towards the boundaries of GM. Conversely, when the normal is orthogonal to the GVF,  $F = 0$  which prevents the model from expanding laterally into the neighboring cortex.

## 2.3. Deformable model design

The second deformable model, which was called “expansion towards cortical boundaries” (ECB), combines FCD features with the GVF motion. The GVF is used to expand the result found with the previous FDM, towards the boundaries of the cortex. The MR features restrict the GVF motion, to prevent the deformable model from progressing into healthy regions. Moreover, the GVF is not taken into account in points which possess MR features of FCD. This ensures that lesional regions segmented by the FDM will not be shrunk by the second deformable model.

The motion of a point  $u$  of the interface  $S$  was then defined as:

$$\begin{aligned} \frac{\partial u}{\partial t} = & \alpha_2 [R_{NL}(u) - R_L(u)] \mathbf{n}_u \\ & + \beta_2 \delta(u) [\hat{\mathbf{v}}(u) \cdot \mathbf{n}_u] \mathbf{n}_u + \epsilon_2 \kappa_u \mathbf{n}_u, \end{aligned} \quad (3)$$

where  $\delta(u) = 1$  if  $R_{NL}(u) > R_L(u)$  and  $\delta(u) = 0$  if  $R_{NL}(u) \leq R_L(u)$ ,  $\alpha_2$ ,  $\beta_2$  and  $\epsilon_2$  are weighting coefficients and  $\kappa_u$ ,  $\mathbf{n}_u$  and  $\hat{\mathbf{v}}(u)$  are defined as in Equations 1 and 2.

$[R_{NL}(u) - R_L(u)] \mathbf{n}_u$  is the same feature-based term that was used in the FDM.  $\delta(u) [\hat{\mathbf{v}}(u) \cdot \mathbf{n}_u] \mathbf{n}_u$  is the GVF-based force defined in Equation 2 and is canceled if  $R_L(u) \geq R_{NL}(u)$ , i.e. if point  $u$  possess the MR features of FCD.

## 2.4. Including transition classes

Since the second deformable model will expand the result of the FDM, it is important to limit as much as possible the false positives in the first model. In particular, the transition classes GM/WM and GM/CSF may be misclassified since their characteristics are closer to those of the lesions. We modified the learning step, which estimates the probabilities  $P(c|f(x))$  (Section 2.1), to take into account these transition classes. The transition between GM and WM was defined by selecting voxels which had a  $3 \times 3 \times 3$  neighborhood composed of at least 30% of GM and 30% of WM, as in the FCD classifier [4]. The GM/CSF transition was computed using a similar process. Then, the learning step was performed on a 6-class map (GM, WM, CSF, L, GM/WM and GM/CSF) instead of the original 4-class map (GM, WM, CSF and L) used in [7]. The definition of  $R_{NL}$  was also modified to take into account five non-lesional classes instead of three.

## 2.5. Level set evolution

The motion equation of the second deformable model was implemented using the level set method [10]. The principle of this method is to define the surface  $S$  as the zero level set of a higher dimensional function  $\phi$ , called the implicit function. To reduce the computational complexity, we used the narrow-band method [10].

Using the derivation from curve motion to level set evolution [10], the ECB can be described by:

$$\begin{aligned} \frac{\partial \phi}{\partial t}(x) = & \alpha_2 [R_{NL}(x) - R_L(x)] |\nabla \phi(x)| \\ & - \beta_2 \delta(x) [\hat{\mathbf{v}}(x) \cdot \nabla \phi(x)] + \epsilon_2 \kappa_x |\nabla \phi(x)| \end{aligned} \quad (4)$$

The level set segmentations were obtained as follows. First, the FCD classifier was used to obtain an initialization for the FDM. The result of the 6-class FDM then constituted the starting point of the ECB whose output defined the segmentation of the FCD lesion. We used the following segmentation parameters:  $\alpha_1 = 0.8$  and  $\epsilon_1 = 0.2$  for the FDM;  $\alpha_2 = 0.2$ ,  $\beta_2 = 0.8$  and  $\epsilon_2 = 0.1$  in the ECB. No fine tuning of the parameters was necessary and the same values were used for all subjects.

## 3. EXPERIMENTS AND RESULTS

### 3.1. Subjects and image preparation

We studied 24 patients (13 males, mean age  $\pm$  SD =  $24 \pm 8$ ) with MRI-visible FCD. The Ethics Board of the Montreal Neurological Institute and Hospital approved the study, and written informed consent was obtained from all participants.

3D MR images were acquired on a 1.5T scanner using a T1-fast field echo sequence with an isotropic voxel size of  $1\text{mm}^3$ . All images underwent automated correction for intensity non-uniformity and intensity standardization, automatic registration into stereotaxic space, brain extraction, and classification of brain tissue in GM, WM and CSF using an histogram-based method with automated threshold [6].

### 3.2. Evaluation strategy

In [7], to assess the performance of the deformable model, we used two sets of manual lesion labels, denoted as  $M_1$  and  $M_2$ , delineated independently on 3D MRI by two trained raters. The mean inter-rater agreement, computed using the similarity index  $S = 2 \frac{|M_1 \cap M_2|}{|M_1| + |M_2|}$ , was 0.62, which corresponds to a substantial agreement. However, the evaluation of the automated segmentation was limited by the remaining differences between the two manual labels.

To overcome this difficulty, we propose here to build ‘‘consensus’’ manual labels, denoted as  $M_C$ . To this purpose, two other observers (NB and AB) jointly inspected the tracings  $M_1$  and  $M_2$  of the two raters and provided a decision for all

ambiguous regions (i.e. regions defined as lesional by one rater but not by the other).

The performance of each of the steps in the procedure (classifier, FDM and ECB) was assessed by comparison with the ‘‘consensus’’ labels  $M_C$ , using the following metrics:

- the aforementioned similarity index  $S = 2 \frac{|A \cap M_C|}{|A| + |M_C|}$  (where  $A$  is the automated segmentation);
- a coverage index  $C = 100 \times |A \cap M_C| / |M_C|$ ;
- a false positive index  $FP = 100 \times |A \setminus M_C| / |A|$ .

### 3.3. Results

The FCD classifier [4] was used to initialize the FDM. It successfully identified the lesion in 18 (18/24=75%) patients. The evaluation was thus done on the 18 detected lesions.

The similarity, coverage, and false positive indices obtained for the ECB, the 6-class FDM (which is used here), the 4-class FDM (proposed in [7]) and the FCD classifier, compared to the consensus manual labels  $M_C$  are reported in Table 1. Segmentation results in three patients with FCD are shown in Figure 2.

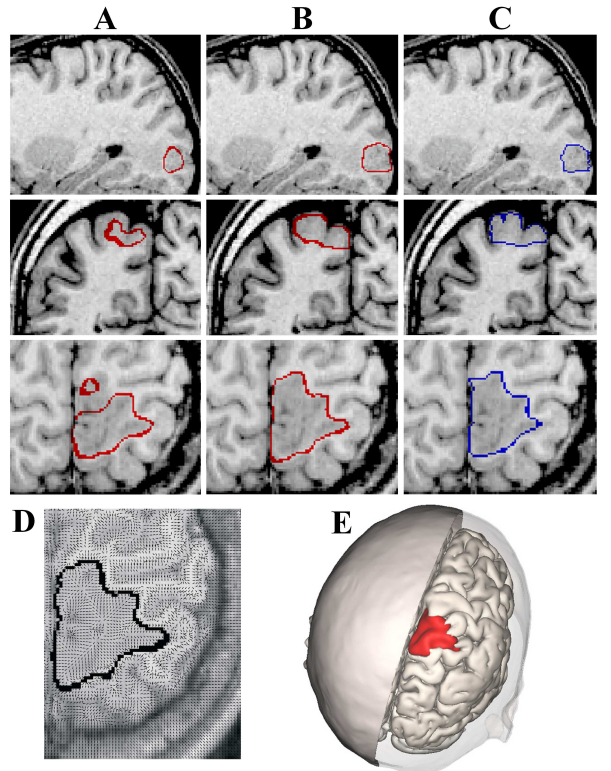


**Fig. 2.** Segmentation results in three patients with FCD. (A) Intermediate results with the 6-class FDM. (B) Final results with the ECB. (C) Consensus labels  $M_C$ . (D) ECB result shown with the GVF. (E) 3D rendering of the ECB result shown with the cortical surface (rendering done with the Anatomist software - <http://www.anatomist.info>).

**Table 1.** Results for the ECB, the FDM (with the 6-class learning and the 4-class learning), and the FCD classifier with respect to the consensus labels  $M_C$ . They are reported as mean $\pm$ SD with the range in parentheses.

	Similarity ( $S$ )	Coverage ( $C$ )	False positives ( $FP$ )
ECB	$0.73 \pm 0.08$ (0.60 to 0.86)	$72\% \pm 16\%$ (44% to 94%)	$20\% \pm 15\%$ (0.4% to 48%)
FDM 6-class	$0.57 \pm 0.17$ (0.22 to 0.77)	$45\% \pm 18\%$ (12% to 71%)	$9\% \pm 10\%$ (0% to 31%)
FDM 4-class	$0.65 \pm 0.13$ (0.4 to 0.82)	$57\% \pm 18\%$ (25% to 81%)	$16\% \pm 12\%$ (0% to 41%)
Classifier	$0.26 \pm 0.14$ (0.05 to 0.46)	$16\% \pm 10\%$ (3% to 30%)	$0.3\% \pm 0.8\%$ (0% to 3.1%)

#### 4. DISCUSSION

In this paper, we proposed and evaluated a method to segment FCD lesions on T1-weighted MRI. We improved our previous feature-based deformable model by introducing a second stage which expands the first result towards the underlying and overlying cortical boundaries, while preventing intracortical motion in the lateral direction. Additionally, we used a modeling of the transition classes GM/WM and GM/CSF which provides a better discrimination between lesions and healthy tissues, thus limiting false positives.

On MRI, FCD lesions possess ill-defined boundaries and are difficult to distinguish from the normal cortex. Their delineation by raters necessarily suffers from subjectivity. For this reason, we introduced “consensus” labels that pool the knowledge of different experts and provide a more objective reference than if separate labels were used.

The level set segmentations achieved a degree of similarity of 0.73 with the consensus labels, which constitutes a strong agreement. Moreover, the deformable model recovered more than 70% of voxels marked as lesional in the labels. The mean false positive index was 20% which constitutes a low value when dealing with small structures such as FCD lesions. Indeed, small objects are penalized by this measure since a small segmentation error can lead to a substantial percentage of false positives. For example, if we consider a sphere which volume is equal to the mean volume of our FCD lesions ( $16.8\text{cm}^3$ ) and as segmentation a sphere which radius is one voxel larger, we obtain  $FP = 17\%$ .

The results also demonstrated the improvement of the second deformable model over the FDM. It provided a substantial enhancement of the lesion coverage while only marginally increasing the false positives, resulting in a stronger overall similarity.

The introduction of transition classes significantly reduced the number of false positives in the FDM. Some lesional areas were also suppressed from the segmentation, resulting in decreased coverage and similarity. However, these areas were recovered by the second deformable model which achieved a higher similarity than the original 4-class FDM.

In conclusion, we proposed a new approach to segment FCD lesions on MRI, improving our previously proposed feature-based deformable model. This segmentation technique

can reduce the subjectivity of lesion delineation and unveil overlooked lesional areas. It may lead to fruitful applications in surgical planning and image-guided surgery.

#### 5. REFERENCES

- [1] D.C. Taylor, M.A. Falconer, et al., “Focal dysplasia of the cerebral cortex in epilepsy,” *J Neurol Neurosurg Psychiatry*, vol. 34, pp. 369–387, 1971.
- [2] S.M. Sisodiya, “Surgery for malformations of cortical development causing epilepsy,” *Brain*, vol. 123, pp. 1075–1091, 2000.
- [3] J. Kassubek, et al., “Detection and localization of focal cortical dysplasia by voxel-based 3-D MRI analysis,” *Epilepsia*, vol. 43, pp. 596–602, 2002.
- [4] S.B. Antel, D.L. Collins, et al., “Automated detection of focal cortical dysplasia lesions using computational models of their MRI characteristics and texture analysis,” *NeuroImage*, vol. 19, no. 4, pp. 1748–59, 2003.
- [5] M. Wilke, J. Kassubek, et al., “Automated detection of gray matter malformations using optimized voxel-based morphometry: a systematic approach,” *NeuroImage*, vol. 20, no. 1, pp. 330–43, 2003.
- [6] S.B. Antel, et al., “Computational models of MRI characteristics of focal cortical dysplasia improve lesion detection,” *NeuroImage*, vol. 17, no. 4, pp. 1755–60, 2002.
- [7] O. Colliot, T. Mansi, N. Bernasconi, V. Naessens, D. Klironomos, and A. Bernasconi, “Segmentation of focal cortical dysplasia lesions using a feature-based level set,” in *Proc. MICCAI 2005*, vol. 3749 of *Lecture Notes in Computer Science*, pp. 375–382, Springer.
- [8] L. Tassi, et al., “Focal cortical dysplasia: neuropathological subtypes, EEG, neuroimaging and surgical outcome,” *Brain*, vol. 125, no. Pt 8, pp. 1719–1732, 2002.
- [9] C. Xu and J.L. Prince, “Snakes, shapes and gradient vector flow,” *IEEE TIP*, vol. 7, no. 3, pp. 359–369, 1998.
- [10] J.A. Sethian, *Level-set methods and fast marching methods*, Cambridge University Press, 2nd edition, 1999.